

Selective and fast plasmon-assisted photo-heating of nanomagnets

Supplementary Information

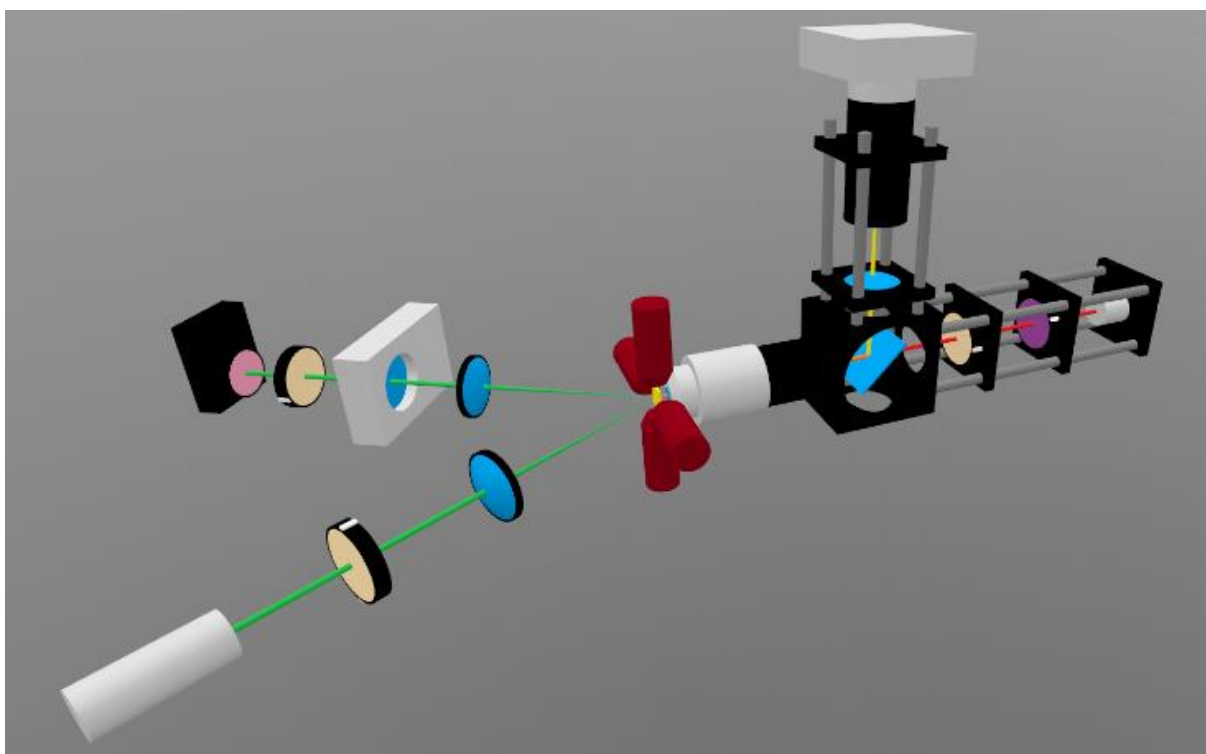
Matteo Pancaldi¹⁺, Naëmi Lao¹, and Paolo Vavassori^{1,2,}*

¹ CIC nanoGUNE, Donostia–San Sebastian E-20018, Spain

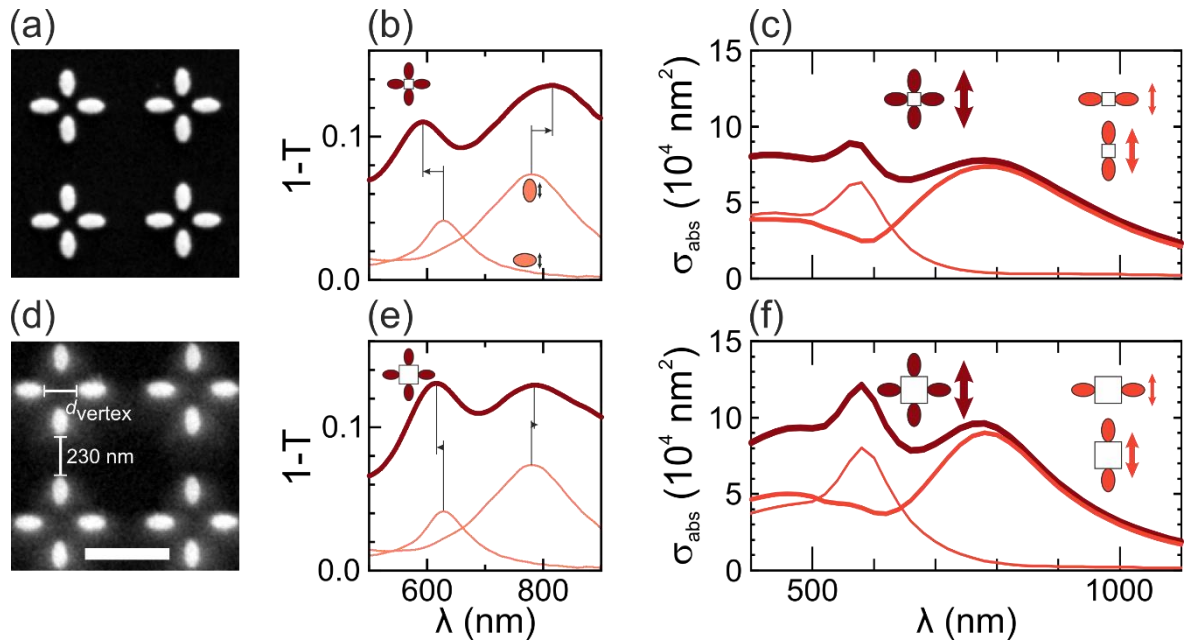
² IKERBASQUE, Basque Foundation for Science, Bilbao E-48013, Spain

⁺ Present address: Department of Physics, Stockholm University, 106 91 Stockholm, Sweden

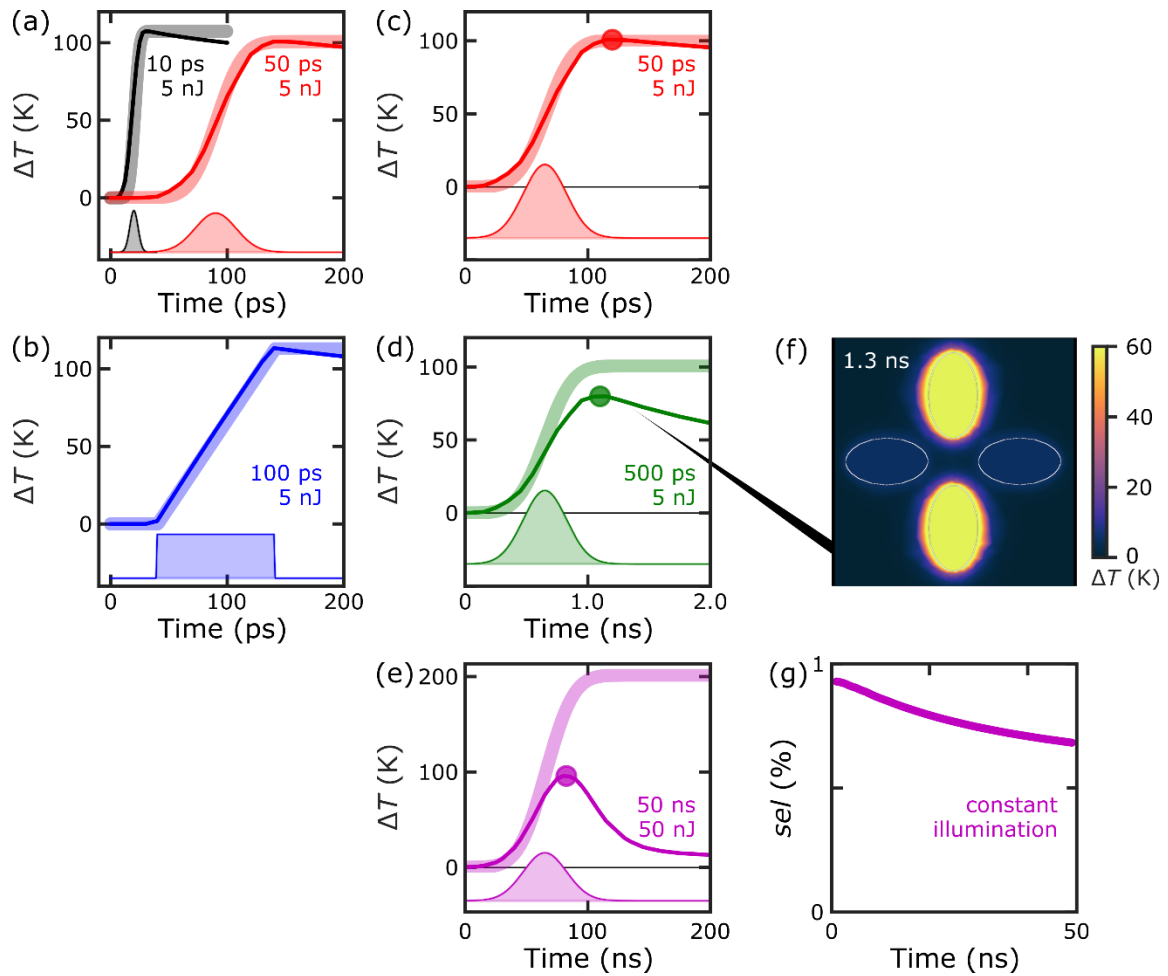
*p.vavassori@nanogune.eu



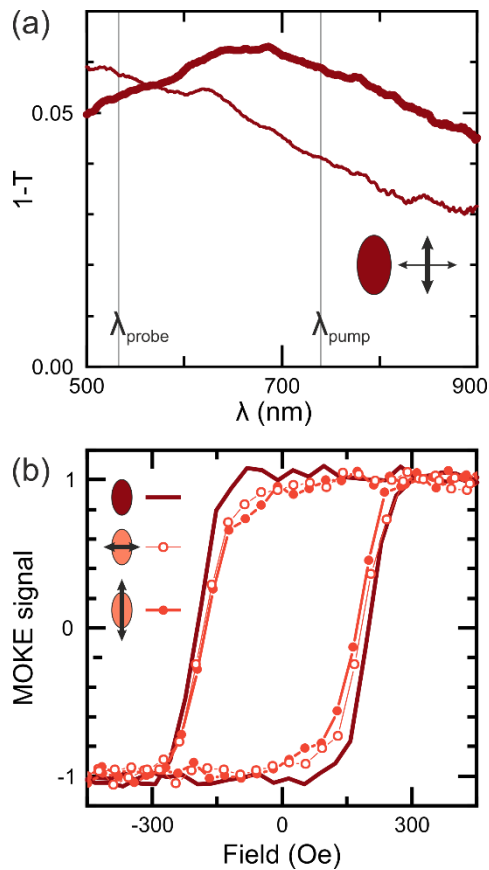
Supplementary Fig S1: Experimental setup. On the left, the MOKE setup (green light path), which probes the samples magnetic response from the front of the substrate, is shown. The sample is situated between magnetic pole shoes (red, middle). The thermoplasmonic excitation with varying light polarization, power, and focus is obtained from the back of the sample (red light path), with the setup shown on the right side of the illustration. A CCD camera allows checking the spatial overlap of the MOKE probe beam coming from the front of the sample (green) and the plasmonic pump beam coming from the back of the sample (red) on the transparent glass sample substrate.



Supplementary Fig S2: Optical properties of 4-vertices. (a,d) SEM micrographs of 4-vertices with perpendicular islands of aspect ratio $AR = 1.75$ ($a_{\text{minor}} = 100$ nm) and a center edge-to-edge islands distance of (a) $d_{\text{vertex}} = 100$ nm, and (d) $d_{\text{vertex}} = 200$ nm. The 4-vertex units are separated by a distance of 230 nm to consider them optically and magnetically isolated (*i.e.* near-field decoupled) from each other. The scale bar in (d) measures 500 μm . (b,e) Experimentally-measured optical extinction spectra $1 - T(\lambda, \mathbf{E})$ show two peaks associated with the two plasmonic resonances along the minor and major ellipse axes of the perpendicular islands of the 4-vertices. Near-field coupling of neighboring islands leads to blue- and redshifts of the plasmon peaks, as indicated. For comparison, the single-island spectra, from Fig. 1(f) scaled by a factor of 0.25, are shown as thin lines (due to the smaller particle surface density S^{-1} the extinction is lower for the vertex arrays than the samples shown in Fig. 1). (c,f) Simulated absorption cross sections $\sigma_{\text{abs}}(\lambda, \mathbf{E})$ for the horizontal pair (thick light red line), vertical pair (thin light red line), and full vertex (solid dark red line).



Supplementary Fig. S3 Time-dependent temperature increase under pulsed illumination. Simulated temperature evolution of a 7x7 lattice of 4-vertices (compare to Fig. 4 and Sec. 5.3.2) illuminated with laser pulses of different shape and duration. (a,b) Under the approximation of quasi-instantaneous plasmonic heating, which is valid for times larger than the electron-phonon relaxation time scale (see main text), the maximum temperature is reached at the end of pulse duration and it is determined by the pulse energy only. The time-dependent temperature increase is proportional to the deposited energy $E_{\text{pulse}}(t)$ via $T(t) \propto \int E_{\text{pulse}}(t) dt$, and thus depends on the pulse shape: (a) For Gaussian pulses, marked here with a solid lines for 10 ps (black) and 50 ps pulses (red), the temperature follows an error function (thick faint lines), whereas (b) for rectangular pulses the temperature increase is linear. (c,-e) For longer time scales, thermal diffusion via the substrate will start to take effect. As the comparison of the effect of Gaussian pulses of (c) 50 ps, (d) 500 ps, and (e) 50 ns shows, the speed of the temperature increase up to the maximum temperature (solid lines) is still proportional to the deposited energy (thick faint lines). In contrast, for longer pulses, the maximum of the time-dependent temperature, marked with a circle, is reached even before the excitation is over, and occurs at lower temperatures as heat is already being transferred to the substrate. (f) For a pulse of 500 ps, the thermal snapshot taken at the time of maximum temperature reveals that heat diffusion extends to the proximity of the heated element, whereas the perpendicular islands still largely remain cool. (g) The effect of sublattice-specific heating, as defined by Eq. (2), reduces under steady-state illumination (here, the constant excitation is switched on at $t = 1$ ns), but retains a high value of around 70 % even after 50 ns.



Supplementary Fig. S4 Plasmonic and magnetic properties of permalloy-only nanomagnets. To show the superior thermoplasmonic properties of gold layers, arrays of permalloy-only nanomagnets with an ellipse aspect ratio $AR=1.75$ ($a_{\text{minor}} = 100$ nm, $a_{\text{major}} = 175$ nm), have been fabricated. (a) Extinction spectra show a weak wavelength- and polarization dependence, and in general a much weaker light-matter interaction compared to the tri-layer Au-Py-Au islands. The pump wavelength $\lambda_{\text{pump}} = 740$ nm (gray line) represent the best compromise between heating efficiency and polarization-dependent selectivity. (b) MOKE hysteresis loops measured under different illumination conditions – no pump (solid line), and a pump beam ($P = 60$ mW) polarized along the ellipse major (closed circles) and minor axis (open circles) – show only a small variation in coercive field ($\Delta H_c < 25$ Oe) and a negligible effect of the light polarization.